ASTROPHYSICS

Gravitational waves from binary supermassive black holes missing in pulsar observations

R. M. Shannon,[1,2]* V. Ravi,[3]* L. T. Lentati,[4] P. D. Lasky,[5] G. Hobbs,[1] M. Kerr,[1] R. N. Manchester,[1] W. A. Coles,[6] Y. Levin,[5] M. Bailes,[3] N. D. R. Bhat,[2] S. Burke-Spolaor,[7] S. Dai,[1,8] M. J. Keith,[9] S. Osłowski,[10,11] D. J. Reardon,[5] W. van Straten,[3] L. Toomey,[1] J.-B. Wang,[12] L. Wen,[13] J. S. B. Wyithe,[14] X.-J. Zhu[13]

Gravitational waves are expected to be radiated by supermassive black hole binaries formed during galaxy mergers. A stochastic superposition of gravitational waves from all such binary systems would modulate the arrival times of pulses from radio pulsars. Using observations of millisecond pulsars obtained with the Parkes radio telescope, we constrained the characteristic amplitude of this background, $A_{c,yr}$, to be $<1.0 \times 10^{-15}$ with 95% confidence. This limit excludes predicted ranges for $A_{c,yr}$ from current models with 91 to 99.7% probability. We conclude that binary evolution is either stalled or dramatically accelerated by galactic-center environments and that higher-cadence and shorter-wavelength observations would be more sensitive to gravitational waves.

Studies of the dynamics of stars and gas in nearby galaxies provide strong evidence for the ubiquity of supermassive ($>10^6$ solar masses) black holes (SMBHs) (*1*). Observations of luminous quasars indicate that SMBHs are hosted by galaxies throughout the history of the universe (*2*) and affect global properties of the host galaxies (*3*). The prevailing dark energy–cold dark matter cosmological paradigm predicts that large galaxies are assembled through the hierarchical merging of smaller galaxies. The remnants of mergers can host gravitationally bound binary SMBHs, with orbits decaying through the emission of gravitational waves (GWs) (*4*).

GWs from binary SMBHs, with periods between ~0.1 and 30 years (*5*), can be detected or constrained by monitoring, for years to decades, a set of rapidly rotating millisecond pulsars (MSPs) distributed throughout our galaxy. Radio emission beams from MSPs are observed as pulses that can be time-tagged with precision as fine as 20 ns (*6*). When traveling across the pulsar-Earth line of sight, GWs induce variations in the arrival times of the pulses (*7*).

The superposition of GWs from the binary SMBH population is a stochastic background (GWB), which is typically characterized by the strain-amplitude spectrum $h_c(f) = A_{c,yr}[f/(1\ \mathrm{year}^{-1})]^{-2/3}$, where f is the GW frequency; $A_{c,yr}$ is the characteristic amplitude of the GWB measured at $f = 1\ \mathrm{year}^{-1}$, predicted to be $>10^{-15}$ (*5*, *8*–*12*); and −2/3 is the predicted spectral index (*5*, *8*–*12*). The GWB is expected to add low-frequency perturbations to pulse arrival times. Although the detection of the GWB would confirm the presence of a cosmological population of binary SMBHs, limits on its amplitude constrain models of galaxy and SMBH evolution (*8*).

As part of the Parkes Pulsar Timing Array (PPTA) project to detect GWs (*6*), we have been monitoring 24 pulsars with the 64-m Parkes radio telescope. Using observations taken at a central wavelength of 10 cm and previously reported methods (*6*, *8*), we have produced a new data set that spans 11 years, which is 3 years longer than previous data sets analyzed at this wavelength. In addition to having greater sensitivity to the GWB than previous data sets because of its longer duration, this new data set was improved by identifying and correcting for some instrumental offsets [supplementary text S1 (*13*)].

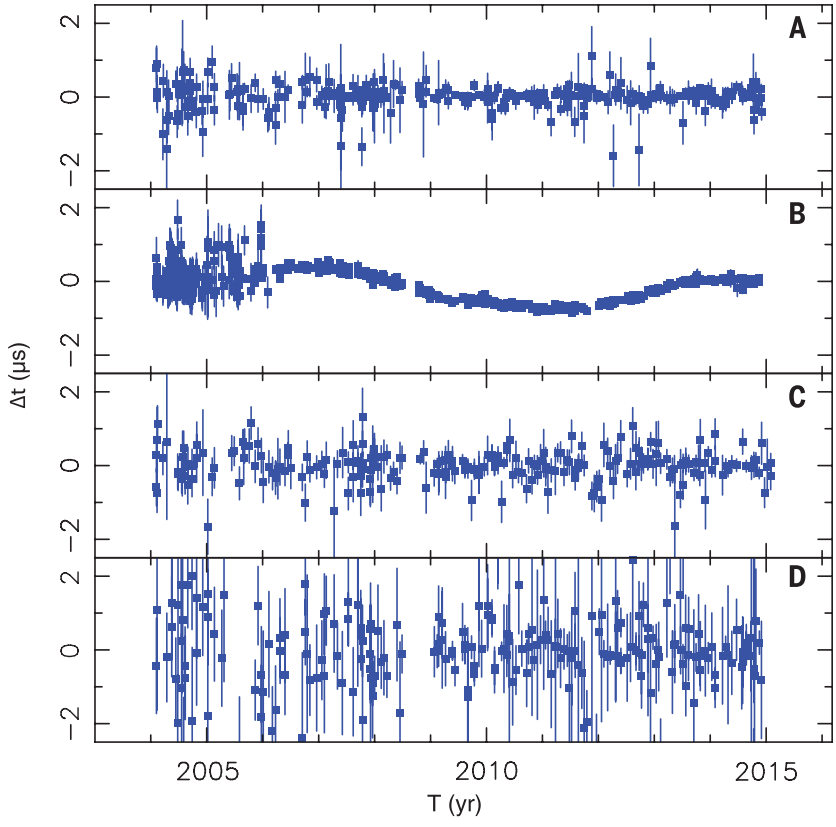

Fig. 1. Residual pulse times of arrival, Δ*t*, for the four pulsars used in our analysis. These include (**A**) PSR J1909-3744, (**B**) PSR J0437-4715, (**C**) PSR J1713+0747, and (**D**) PSR J1744-1134.

[1]Commonwealth Science and Industrial Research Organization (CSIRO) Astronomy and Space Science, Australia Telescope National Facility, Post Office Box 76, Epping, New South Wales 1710, Australia. [2]International Centre for Radio Astronomy Research, Curtin University, Bentley, Western Australia 6102, Australia. [3]Centre for Astrophysics and Supercomputing, Swinburne University of Technology, Post Office Box 218, Hawthorn, Victoria 3122, Australia. [4]Astrophysics Group, Cavendish Laboratory, JJ Thomson Avenue, Cambridge CB3 0HE, UK. [5]Monash Centre for Astrophysics, School of Physics and Astronomy, Monash University, Post Office Box 27, Victoria 3800, Australia. [6]Department of Electrical and Computer Engineering, University of California–San Diego, La Jolla, CA 92093, USA. [7]National Radio Astronomical Observatory, Array Operations Center, Post Office Box 0, Socorro, NM 87801-0387, USA. [8]Department of Astronomy, School of Physics, Peking University, Beijing 100871, China. [9]Jodrell Bank Centre for Astrophysics, University of Manchester, Manchester M13 9PL, UK. [10]Department of Physics, Universitat Bielefeld, Universitatsstrasse 25, D-33615 Bielefeld, Germany. [11]Max-Planck-Institut für Radioastronomie, Auf dem Hügel 69, 53121 Bonn, Germany. [12]Xinjiang Astronomical Observatory, Chinese Academy of Sciences, 150 Science 1-Street, Urumqi, Xinjiang 830011, China. [13]School of Physics, University of Western Australia, Crawley, Western Australia 6009, Australia. [14]School of Physics, University of Melbourne, Parkville, Victoria 3010, Australia.
*Corresponding author. E-mail: ryan.shannon@csiro.au (R.S.); v.vikram.ravi@gmail.com (V.R.)

We searched for the GWB in observations of the four pulsars (Fig. 1) that have the highest timing precision and therefore would be most sensitive to it. Observations of these pulsars at other wavelengths contain excess noise that is inconsistent with the 10-cm observations, and they were therefore excluded from this analysis (supplementary text S2.1). This exclusion does not bias our analysis, because GWs produce achromatic variations in arrival times. Observations of other pulsars are not presented here because they have insufficient timing precision, relative to the best pulsars, to influence the search (supplementary text S2). We also have not corrected for chromatic arrival-time variations associated with propagation through a varying column of interstellar plasma, because these effects are small in the 10-cm band (*14*). Additionally, using uncorrected observations can only have reduced our sensitivity to the GWB, making our analysis conservative.

We used a Bayesian methodology (*15*) to marginalize over the pulsar rotational ephemerides and to search for stochastic contributions to the arrival times. The stochastic terms include excess white noise associated with intrinsic pulse-shape changes and instrumental distortions uncorrelated between observations. They also include excess low-frequency timing noise that is uncorrelated between pulsars, which could be intrinsic to the pulsars or caused by interstellar propagation effects. In addition, the model includes the GWB, which produces timing perturbations that are correlated between the pulsars (*7*). The methodology also enables us to quantitatively compare models by providing evidence, in the form of a probability,

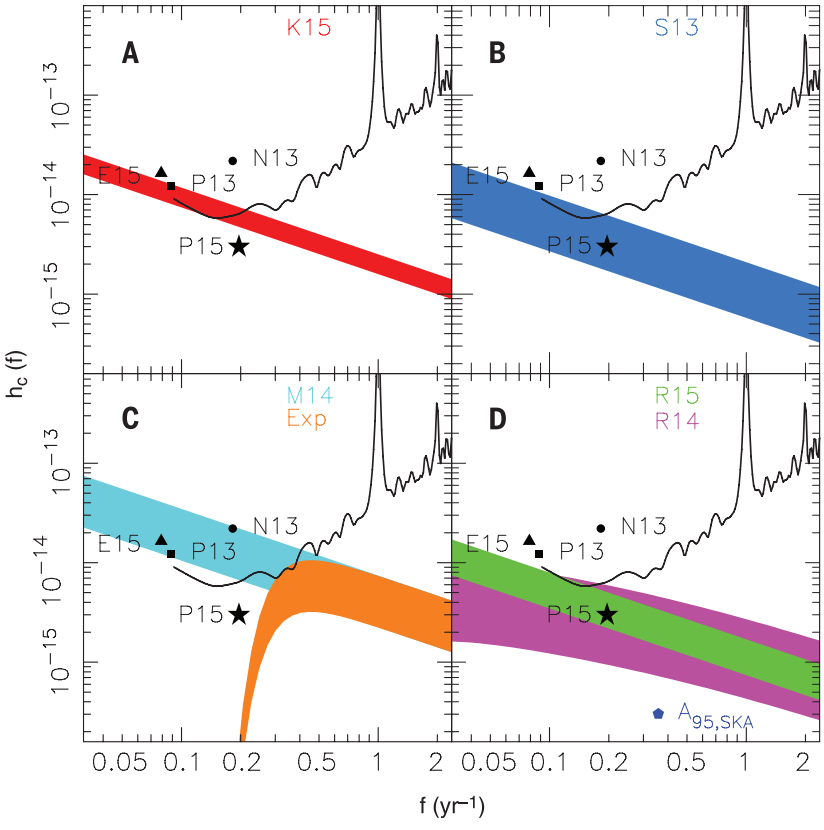

Fig. 2. Predictions and limits on the GWB strain spectrum. The black stars (labeled P15) show the 95% confidence limit that we obtained, assuming $h_c(f) = A_{c,yr}[f/(1\ year^{-1})]^{-2/3}$. The other symbols show previously published limits from the European Pulsar Timing Array (triangles labeled E15) (*20*), the North American Nanohertz Observatory for Gravitational Waves collaboration (circles labeled N13) (*29*), and our previous limit (squares labeled P13) (*8*). Each panel shows a different prediction for the GWB, based on four models for SMBH evolution that predict a power-law form for $h_c(f)$: (**A**) K15 (*12*), (**B**) S13 (*9*), (**C**) M14 (*10*), and (**D**) R15 (*11*). Predictions are shown as shaded regions (correspondingly colored) that represent the 1σ uncertainty. Also shown in (C) and (D) are models Exp (supplementary text S2.2) and R14 (*22*), respectively, which include the effects of environmentally driven binary evolution and therefore predict more complex strain spectra. The black curve in each panel shows the nominal single-frequency sensitivities of our observations (supplementary text S2.2), and it is above our limit because of the statistical penalties applied when searching individual frequencies. In (D), the blue pentagon (labeled $A_{95,SKA}$) shows the projected upper limit on $A_{c,yr}$ obtained by a single-pulsar timing campaign conducted with a next-generation radio telescope (the SKA) (supplementary text S2.2); it excludes all considered models with > 98% probability.

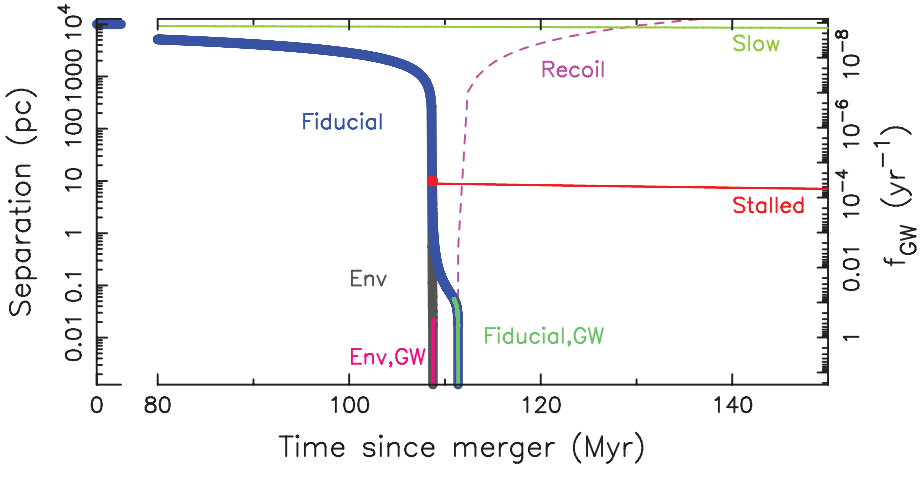

Fig. 3. Illustrative evolutionary paths for a pair of 10^9–solar-mass SMBHs in a galaxy merger. The figure shows the pair separation and the GW emission frequency f_{GW}, assuming the binary is in a circular orbit. The blue curve shows the evolution of the separation of the SMBHs using fiducial assumptions, which results in a GWB that is inconsistent with our data. The cyan curve (labeled Fiducial, GW) is the portion of the evolution that occurs when GW emission dominates orbital decay. We also show scenarios that could explain our GWB limit. First, the galaxy merger rate could be lower, as represented by the slow merger curve (green). Alternatively, after the SMBHs form a binary (red circle), the orbital evolution may stall before emitting GWs (red curve). The gray curve (labeled Env) shows a scenario in which a dense binary SMBH environment drives orbital decay through the GW frequency band at which our observations are sensitive. In this case, GW emission dominates only for $f_{GW} > 0.5\ year^{-1}$ (pink curve labeled Env,GW). Last, it is possible that the post-coalescence SMBH could undergo gravitational recoil and escape its host galaxy (purple dashed curve), negating the possibility of it forming a binary SMBH again. Myr, millions of years.

that can be used to select a preferred model (supplementary text S2).

We found no evidence for the GWB in our data set. We therefore placed an upper limit on the amplitude of the GWB by analyzing its posterior distribution. The pulsar that individually provides the best limit on the GWB, PSR J1909–3744 (Fig. 1), shows no evidence for excess low-frequency timing noise. The pulsar that provides the third-most constraining limit, PSR J0437-4715 (Fig. 1), shows evidence for a low-frequency signal that is inconsistent both with the predicted GWB spectral shape (99.0% probability) and, in amplitude, with the limit derived from PSR J1909–3744 (99.4% probability).

For the power-law GWB strain-amplitude spectrum, we found $A_{c,yr}$ to be $<1.0 \times 10^{-15}$ with 95% probability (Fig. 2). This corresponds to an upper limit on the fractional closure density of the universe (Ω_{GW}) of 2.3×10^{-10} at a frequency of 0.2 year^{-1} (supplementary text S2.2). This is a factor of 6 lower than any previous limit (Fig. 2). Other pulsar timing array experiments with comparable data spans, but with longer-wavelength observations, do not achieve the same sensitivity to GWs (*16*) because of the higher timing precision in our observations and the presence of low-frequency noise in theirs. Our data are inconsistent with current models for the GWB (*9*–*12*) with between 91 and 99.7% probability (*13*).

Our results therefore suggest that at least one of the physical assumptions underlying these GWB models are incorrect. Models for the binary SMBH population rely on measurements of the galaxy merger rate. They also assume that all galaxy mergers form binary SMBHs that coalesce well before a subsequent galaxy merger, and that binary orbital decay is driven only by losses of energy to GWs when radiating in the pulsar-timing frequency band (Fig. 3, black curve).

Figure 3 shows schematically the evolution of a binary SMBH, in which each component has a mass of 10^9 solar masses, evolving under standard assumptions (Fig. 3, blue curve) and in other ways that produce a weaker GWB.

Longer galaxy-merger time scales would result in a lower inferred merger rate (Fig. 3, green curve), fewer binary SMBHs, and hence a lower GWB amplitude. Although predictions for merger time scales vary by a factor of 3 (*17*), models that include this uncertainty (*9*, *11*) are in tension with our limit. Shorter predicted time scales result from the inclusion of more sophisticated physical mechanisms and are therefore favored (*17*). Therefore, galaxy mergers are expected to rapidly form gravitationally bound binaries.

Models for the GWB also assume that all large galaxies host SMBHs. A low SMBH-occupation fraction beyond the local universe (redshifts $z > 0.3$) could result from exceedingly rare, high-redshift SMBH-seed formation (*18*). For this to be the case, seed SMBHs would have to occupy ~1% of the most massive galaxies at $z \sim 6$ (*19*). The models also assume that, post-coalescence, SMBHs remain gravitationally bound to their host galaxies. However, it is unlikely that the acceleration of post-coalescence SMBHs beyond galactic escape velocities through gravitational-radiation recoil (Fig. 3, purple dashed curve) results in a substantial number of galaxies without central SMBHs (*20*).

The GWB amplitude would also be reduced if SMBH binaries do not efficiently reach the GW-emitting stage (Fig. 3, red curve). Dynamical friction is expected to bring the SMBHs in a merging galaxy pair close enough to form a bound binary (*4*), with an orbital major axis $a_{form} \sim 60\, M_9^{0.54}$ pc, where M_9 is the mass of the larger SMBH in units of 10^9 solar masses (supplementary text S4). The time to coalescence through GW emission is $t_{GW} = 18\, M_9^{-3}[a_{form}/(1\text{ pc})]^4$ billion years in the lower-limiting case of an equal-mass binary, which is longer than the age of the universe. Hence, another mechanism in addition to GW emission is required to drive binaries to coalescence.

Observations and theoretical models, however, indicate that binary SMBHs can coalesce within the age of the universe through the coupling of binary SMBHs to their environments (*21*). Proposed coupling mechanisms include the three-body scattering of stars on radial orbits and viscous friction against circumbinary gas. The actions of environments (Fig. 3, gray curve) would cause binaries to spend less time emitting GWs, reducing the GWB amplitude at low frequencies. Our nondetection of the GWB may therefore result from the efficient coupling of binary SMBHs to their environments (*10*, *22*, *23*).

Modeling of the stellar environments of the cosmological population of binary SMBHs (*22*) indicates that the GWB characteristic-strain spectrum may be attenuated at frequencies up to 0.3 year^{-1} (Fig. 2); similar results are obtained when the possible gas-rich environments of binary SMBHs are considered (*23*). Our GWB constraint, placed at 0.2 year^{-1}, is consistent with some models that predict the extreme efficiency of environments in shrinking SMBH binary orbits (model R14, Fig. 2). However, other environmentally driven models that include higher galaxy merger rates (*10*) are inconsistent with our limit (model Exp, Fig. 2)

Distinguishing between explanations for our limit requires further observations and better models of SMBH evolution. The characterization of a substantial population of binary or recoiling SMBHs (*24*) would better delineate the coalescence rate. The coalescence events themselves may produce strong millihertz-frequency GWs that could be detected by space-based laser interferometers (*5*). The detection of the GWB at frequencies $\gtrsim$0.2 year^{-1} with the currently predicted amplitude would provide strong evidence for the high efficiency of binary environments in shrinking orbits (*25*). This hypothesis also predicts an enhanced prospect for detecting low-frequency GWs from the most massive individual binary SMBHs, which are less affected by their environments (*22*, *23*). The alternate explanation for our limit is that the rate of coalescence between SMBHs is lower than current estimates suggest; in this case, the GWB may still have a power-law spectrum.

This limit implies that a change in observational strategy could increase the sensitivity of pulsar timing arrays to GWs. One approach is to obtain more observations of pulsars with comparable sensitivity to those of our four best pulsars. If the observed excess noise at longer radio wavelengths is astrophysical, observations will need to be conducted at shorter wavelengths ($\lesssim$10 cm). In this case, GWB detection may require observations with a sensitive radio telescope such as the Square Kilometre Array [SKA (*26*)], because MSP emission is weaker at these wavelengths. If binary SMBH environments are driving orbital evolution, a high-cadence campaign is required to detect the GWB at frequencies $\gtrsim$0.2 year^{-1}. Alternatively, the GWB could have a power-law spectrum but be weak in amplitude. Our limit implies that there is a 50% probability that $A_{c,yr} < 2.4 \times 10^{-16}$. If this is the case, the first evidence for the GWB will be low-frequency perturbations to timing observations of the most stable pulsar, PSR J1909–3744, when longer data spans are achieved. In all cases, the predicted time to detection of the GWB with pulsar timing arrays (*27*) has been underestimated.

It is also possible that there is a more exotic reason for our nondetection. We have not yet tested GWBs expected from alternate theories of gravity. Our limit is consistent with GWs being absorbed on cosmological scales (*28*). Until GWs are detected, our limits will continue to improve with data span, as more pulsars are added into the sample and improved data analysis methods are developed (Fig. 2, blue pentagon). These limits will provide even stronger constraints on models of SMBH formation and evolution.

REFERENCES AND NOTES

1. J. Kormendy, L. Ho, *Annu. Rev. Astron. Astrophys.* **51**, 511–653 (2013).
2. F. Shankar, D. H. Weinberg, J. Miralda-Escudé, *Mon. Not. R. Astron. Soc.* **428**, 421–446 (2013).
3. A. Fabian, *Annu. Rev. Astron. Astrophys.* **50**, 455–489 (2012).
4. M. Begelman, R. Blandford, M. Rees, *Nature* **287**, 307–309 (1980).
5. J. S. B. Wyithe, A. Loeb, *Astrophys. J.* **590**, 691–706 (2003).
6. R. N. Manchester *et al.*, *Publ. Astron. Soc. Aust.* **30**, e017 (2013).
7. R. W. Hellings, G. S. Downs, *Astrophys. J.* **265**, L39 (1983).
8. R. M. Shannon *et al.*, *Science* **342**, 334–337 (2013).
9. A. Sesana, *Class. Quantum Gravity* **30**, 224014 (2013).
10. S. T. McWilliams, J. P. Ostriker, F. Pretorius, *Astrophys. J.* **789**, 156 (2014).
11. V. Ravi, J. S. B. Wyithe, R. M. Shannon, G. Hobbs, *Mon. Not. R. Astron. Soc.* **447**, 2772–2783 (2015).
12. A. Kulier, J. P. Ostriker, P. Natarajan, C. N. Lackner, R. Cen, *Astrophys. J.* **799**, 178 (2015).
13. Supplementary materials are available on *Science* Online.
14. M. J. Keith *et al.*, *Mon. Not. R. Astron. Soc.* **429**, 2161–2174 (2013).
15. L. Lentati *et al.*, *Phys. Rev. D Part. Fields Gravit. Cosmol.* **87**, 104021 (2013).
16. L. Lentati *et al.*, *Mon. Not. R. Astron. Soc.* **453**, 2576–2598 (2015).
17. C. Conselice, *Annu. Rev. Astron. Astrophys.* **52**, 291–337 (2014).
18. K. Menou, Z. Haiman, V. K. Narayanan, *Astrophys. J.* **558**, 535–542 (2001).
19. T. L. Tanaka, *Class. Quantum Gravity* **31**, 244005 (2014).
20. A. Gerosa, A. Sesana, *Mon. Not. R. Astron. Soc.* **446**, 38–55 (2015).
21. M. Colpi, *Space Sci. Rev.* **183**, 189–221 (2014).
22. V. Ravi, J. S. B. Wyithe, R. M. Shannon, G. Hobbs, R. N. Manchester, *Mon. Not. R. Astron. Soc.* **442**, 56–68 (2014).
23. B. Kocsis, A. Sesana, *Mon. Not. R. Astron. Soc.* **411**, 1467–1479 (2011).
24. M. Eracleous, T. A. Boroson, J. P. Halpern, J. Liu, *Astrophys. J.* **201**, 23 (2012).
25. L. Sampson, N. J. Cornish, S. T. McWilliams, *Phys. Rev. D Part. Fields Gravit. Cosmol.* **91**, 084055 (2015).
26. G. H. Janssen *et al.*, in *Advancing Astrophysics with the Square Kilometer Array*, T. L. Bourke *et al.*, Eds. (Proceedings of

Science, Trieste, Italy, 2015); http://pos.sissa.it/archive/conferences/215/037/AASKA14_037.pdf.
27. X. Siemens, J. Ellis, F. Jenet, J. D. Romano, *Class. Quantum Gravity* **30**, 224015 (2013).
28. S. W. Hawking, *Astrophys. J.* **145**, 544 (1966).
29. P. B. Demorest *et al.*, *Astrophys. J.* **762**, 94 (2013).

ACKNOWLEDGMENTS

We thank the observers, engineers, and Parkes Observatory staff members who have assisted with the observations reported in this paper. We thank R. van Haasteren for assistance with the use of the code *piccard*, E. Thomas for comments on the manuscript, and I. Mandel for discussions on model selection. The Parkes radio telescope is part of the Australia Telescope National Facility, which is funded by the Commonwealth of Australia for operation as a National Facility managed by CSIRO. The PPTA project was initiated with support from R.N.M.'s Australian Research Council (ARC) Federation Fellowship (grant FF0348478) and from CSIRO under that fellowship program. The PPTA project has also received support from ARC through Discovery Project grants DP0985272 and DP140102578. N.D.R.B. acknowledges support from a Curtin University research fellowship. G.H. and Y.L. are recipients of ARC Future Fellowships (respectively, grants FT120100595 and FT110100384). S.O. is supported by the Alexander von Humboldt Foundation. R.M.S. acknowledges travel support from CSIRO through a John Philip Award for excellence in early-career research. The authors declare no conflicts of interest. Data used in this analysis can be accessed via the Australian National Data Service (www.ands.org.au).

SUPPLEMENTARY MATERIALS

www.sciencemag.org/content/349/6255/1522/suppl/DC1
Supplementary Text
Figs. S1 to S2
Tables S1 to S8
References (*30*–*54*)

26 March 2015; accepted 12 August 2015
10.1126/science.aab1910

BIOCATALYSIS

Conversion of alcohols to enantiopure amines through dual-enzyme hydrogen-borrowing cascades

Francesco G. Mutti,[1,2]*† Tanja Knaus,[2]† Nigel S. Scrutton,[2] Michael Breuer,[3] Nicholas J. Turner[1]*

α-Chiral amines are key intermediates for the synthesis of a plethora of chemical compounds at industrial scale. We present a biocatalytic hydrogen-borrowing amination of primary and secondary alcohols that allows for the efficient and environmentally benign production of enantiopure amines. The method relies on a combination of two enzymes: an alcohol dehydrogenase (from *Aromatoleum* sp., *Lactobacillus* sp., or *Bacillus* sp.) operating in tandem with an amine dehydrogenase (engineered from *Bacillus* sp.) to aminate a structurally diverse range of aromatic and aliphatic alcohols, yielding up to 96% conversion and 99% enantiomeric excess. Primary alcohols were aminated with high conversion (up to 99%). This redox self-sufficient cascade possesses high atom efficiency, sourcing nitrogen from ammonium and generating water as the sole by-product.

Amines are among the most frequently used chemical intermediates for the production of active pharmaceutical ingredients, fine chemicals, agrochemicals, polymers, dyestuffs, pigments, emulsifiers, and plasticizing agents (*1*). However, the requisite amines are scarce in nature, and their industrial production mainly relies on the metal-catalyzed hydrogenation of enamides (i.e., obtained from related ketone precursors). This process requires transition metal complexes, which are expensive and increasingly unsustainable (*2*). Moreover, the asymmetric synthesis of amines from ketone precursors requires protection and deprotection steps that generate copious amounts of waste. As a consequence, various chemical processes for the direct conversion of alcohols into amines have been developed during the past decade. The intrinsic advantage of the direct amination of an alcohol is that the reagent and the product are in the same oxidation state; therefore, theoretically, additional redox equivalents are not required. However, many of these methods have low efficiency and high environmental impact (e.g., Mitsunobu reaction) (*3*). The amination of simple alcohols such as methanol and ethanol via heterogeneous catalysis requires harsh conditions (>200°C), and more structurally diverse alcohols are either converted with extremely low chemoselectivity or not converted at all (*4*). Furthermore, most of the work in this field involves nonchiral substrates, whereas 40% of the commercial optically active drugs are chiral amines (*2*). Increasingly, biocatalytic methods are applied for the production of optically active amines [e.g., the lipase-catalyzed resolution of racemic mixtures of amines or the ω-transaminase process; a recent example uses an engineered enzyme applied to the industrial manufacture of the diabetes medication Januvia (sitagliptin)] (*5*–*7*).

Multistep chemical reactions in one pot avoid the need for isolation of intermediates and purification steps. This approach offers economic as well as environmental benefits, because it eliminates the need for time-consuming intermediate work-ups and minimizes the use of organic solvents for extraction and purification as well as energy for evaporation and mass transfer (*8*). As a consequence, cascade reactions generally possess elevated atom efficiency and potentially lower environmental impact factors (*9*). The major challenge is to perform cascade reactions wherein an oxidative and a reductive step are running simultaneously. Even more challenging is to carry out a simultaneous interconnected redox-neutral cascade wherein the electrons liberated in the first oxidative step are quantitatively consumed in the subsequent reductive step [(*8*); for a recent detailed study, see (*10*)]. This concept is the basis for the hydrogen-borrowing conversion of alcohols (primary or secondary) into amines. The reducing equivalents (i.e., hydride) liberated in the first step—the oxidation of the alcohol to the ketone—are directly consumed in the second interconnected step—reductive amination of the ketone.

A number of chemocatalytic hydrogen-borrowing methods have recently been developed using ruthenium as well as iridium catalysts (*11*, *12*). However, the required reaction conditions (e.g., high catalyst and cocatalyst loading, low substrate concentration, moderate chemoselectivity, moderate or total lack of stereoselectivity, the requirement of an excess of substrate, and stringent temperature and elevated pressure requirements) complicate the application of these methods on a large scale (*13*). Another recently developed hydrogen-borrowing chemical method involves the stoichiometric use of Ellman's enantiopure sulfinamide auxiliary as the nitrogen donor in combination with a Ru-Macho catalyst (*14*). Besides the requirement of the expensive chiral auxiliary, the maximum diastereomeric excess was 90%. A reported biocatalytic hydrogen-borrowing amination of alcohols combining three enzymes—a ω-transaminase (ωTA), an alcohol dehydrogenase (ADH), and the alanine dehydrogenase from *Bacillus subtilis* (AlaDH)—also lacks efficiency because of the requirement for at least 5 equivalents of L- or D-alanine as the sacrificial amine donor and also as a result of the lower conversion and chemoselectivity for the amination of secondary alcohols (*15*, *16*). Another redox-neutral biocatalytic cascade was applied for the deracemization of mandelic acid to enantioenriched L-phenylglycine. However, the method was limited to the conversion of this specific α-hydroxy acid (*17*).

Here, we present a highly enantioselective catalytic hydrogen-borrowing amination of primary

[1]School of Chemistry, University of Manchester, Manchester Institute of Biotechnology, Manchester M1 7DN, UK. [2]Manchester Institute of Biotechnology, Faculty of Life Sciences, University of Manchester, Manchester M1 7DN, UK. [3]BASF SE, White Biotechnology Research, GBW/B-A030, 67056 Ludwigshafen, Germany.
***Corresponding author. E-mail: nicholas.turner@manchester.ac.uk (N.J.T.); f.mutti@uva.nl (F.G.M.)** †Present address: Van 't Hoff Institute for Molecular Sciences, University of Amsterdam, Science Park 904, 1098 XH Amsterdam, Netherlands.

Gravitational waves from binary supermassive black holes missing in pulsar observations

R. M. Shannon *et al.*

Science **349**, 1522 (2015);
DOI: 10.1126/science.aab1910